Differential Cross Sections for the Production of Protons in the Reactions of ~160-MeV Protons on Nuclei*

R. W. PEELLE, T. A. LOVE, N. W. HILL, AND R. T. SANTORO
Oak Ridge National Laboratory, Oak Ridge, Tennessee
(Received 21 August 1967)

Cross sections differential in both angle and energy were obtained by flight-time spectrometry for secondary protons above 20 MeV from 158-MeV protons on Be, C, H_2O, Al, Co, and Bi targets. Enough angles were studied to present rough angular distributions from aluminum and cobalt. All secondary charged particles were assumed to be protons, for which the energy resolution varied from 25 to 50%. The observed differential cross sections change smoothly with angle and target mass, and show no peak corresponding to quasifree scattering near the energy corresponding to free nucleon-nucleon scattering. The measurements are compared with others available at the same incident energy and with estimates based on intranuclear-cascade-plus-evaporation calculations. The observed cross sections are larger than the estimated ones at angles of 90° and 120°, and at low energies for angles more forward than 45°. At 60°, the observed cross sections are in accord with the Monte Carlo estimates.

I. INTRODUCTION

THE differential nucleon-production cross sections for 0.1- to 1-BeV nucleons on complex nuclei have not been thoroughly studied in the secondary nucleon-energy regions well below the elastic scattering. This paper reviews the information and ideas pertinent to the less energetic regions of the secondary spectra and presents an experiment which measured some differential cross sections for secondary protons above 20 MeV from 158 MeV protons on nuclei. The experiment utilized low-resolution flight-time spectroscopy because the experimental arrangement was derived from one designed to observe the corresponding secondary neutrons.

The cross sections discussed here are for production of a secondary proton per unit solid angle and energy, written $\sigma_{p,xpy}(E; E',\theta)$, regardless of any production of other radiations in the same interaction.[1] If this cross section is integrated over all solid angle and all secondary energies E', the result is the nonelastic cross section times the average secondary-proton multiplicity in nonelastic reactions induced by protons of energy E. The resolution of our spectrometer was inadequate for resolving elastic scattering, so that at small scattering angles θ, where elastic scattering is intense, we did not quite measure $\sigma_{p,xpy}(\theta)$.

An incident nucleon with kinetic energy greater than 0.1 BeV is now usually treated in the approximation that it interacts initially with a single target nucleon.[2] This view is encouraged by the incident nucleon's short wavelength and moderately long free path in the nucleus, as well as by the success of the notion. If neither resulting nucleon reacts again, the reaction is termed a pure quasifree knockout scattering event. Even if secondary or tertiary intranuclear reactions occur, the free-particle n-p and p-p interactions are thought to dominate as long as the reaction products are energetic. When the momentum transfer is small, low-lying states of the residual nucleus may be excited in what are generally considered nuclear rather than nucleon direct reactions.

When the sequence of quasifree interactions (intranuclear cascade) is complete, one often assumes that the nucleus is uniformly "heated," so that a nucleon-evaporation process can occur; however, the process of energy distribution is being reexamined.[3] In any case, the mean residual nuclear excitation from cascade processes should be a slowly varying function of the incident energy. Nucleon spectra at low energies from incident protons in the range 160–190 MeV show even for low-A targets the qualitative features expected from nucleon-evaporation spectra.[4–7]

In the central regions of the emitted-particle spectra where quasifree scattering would appear at energies averaging a little below $E\cos^2\theta$,[8] broadened by the target-nucleon-momentum distribution as well as by failures of the single-quasifree-scattering approximation, the data are qualitatively less consistent. Yet this region should contain a large share of the secondary energy, as well as a large share of the particles from light-nuclide targets. At high energies and small angles, the peak from quasifree scattering was apparent in carbon in the experiment of Cladis, Hess, and Moyer,[9] who observed it at 30° and 40° for incident 340-MeV protons. Prominent quasifree-scattering peaks have also been seen for

* Research sponsored by the National Aeronautics and Space Administration under Union Carbide Corporation's contract with the U. S. Atomic Energy Commission.

[1] The cross-section notation employed was introduced by C. D. Zerby and H. Goldstein, Oak Ridge National Laboratory Report No. ORNL-3499, 1963, Vol. II, pp. 63–66 (unpublished).

[2] Perhaps first suggested in the current context by R. Serber, Phys. Rev. **72**, 114 (1947).

[3] J. Griffin, Phys. Rev. Letters **17**, 478 (1966).

[4] D. M. Skyrme and W. S. C. Williams, Phil. Mag. **42**, 1187 (1951).

[5] C. Edward Gross, University of California Radiation Laboratory Report No. UCRL-3330, 1956 (unpublished).

[6] R. Fox and N. Ramsey, Phys. Rev. **125**, 1609 (1962).

[7] L. Evan Bailey, University of California Radiation Laboratory Report No. UCRL-3334, 1956 (unpublished).

[8] Both the relativistic effects and the average nuclear potential act to reduce the energy of any quasifree-scattering peak in the nucleon spectrum.

[9] J. B. Cladis, W. N. Hess, and B. J. Moyer, Phys. Rev. **87**, 425 (1952).

outgoing protons from incident 650-MeV protons.[10] Strong, broad high-energy neutron peaks often ascribed to quasifree scattering have been seen at extreme forward angles at incident energies of 140–240 MeV.[11–13] Spectrum characteristics indicating quasifree scattering have been obscure in results at lower incident energies. Strauch and Titus[14] did not see evidence of quasifree scattering in the emerging proton spectrum at 90-MeV incident proton energy for any element at 40° or for carbon at any angle. Similarly, Hofmann and Strauch,[15] in studying neutrons from 90-MeV protons, saw no quasifree-scattering peak at any angle, except for D, Be, and Li targets at small angles. Protons early observed at 90° from incident 240-MeV protons on carbon[16] had intensity strong enough and energy high enough to either confirm the presence of very high momentum components in the nucleus, if single quasifree scattering dominates, or emphasize the importance of more complex interactions.

Turning to secondary charged particles in the 160-MeV incident energy region directly of interest, Wall and Roos[17] measured the quasifree scattering for a number of elements above their counter threshold of about 40 MeV, and found broad peaks in the scattered spectra for all elements, at least for angles below 60°. It will be seen that these data, which are supported somewhat by the work of Genin *et al.*[18] for gold and by Radvanyi and Genin[19] for carbon, are in conflict with the present experiment. Bailey[7] observed a slight minimum in his spectra covering the 0–65° angle range from Na and Al, but not from Ag. Dahlgren *et al.*,[20] using 185-MeV incident protons, studied secondary-proton spectra above 20 MeV at angles of 60°–100° and saw no quasifree-scattering peak, except possibly at their smallest angles. Energetic deuterons, tritons, and other particles are observed[17–23] in the emerging spectra with a combined intensity relative to protons of 10–20%.

How may we understand qualitatively the emerging proton spectra at energies well below the elastic scattering but above the evaporation region? For favorable energies and angles, Born-approximation estimates on the basis of a single collision have been made to relate the peak of the quasifree-scattered spectrum to the nuclear-momentum distribution, but detailed calculation of expected spectra extending to lower energies has been obtained from only the cascade-plus-evaporation model discussed below.

The intranuclear-cascade model was introduced by Goldberger[24] and first extensively used by Metropolis *et al.*[25] Monte Carlo techniques are used to follow the incident "nucleon" and its microscopic reaction products along classical paths through a model nucleus which is a bundle of moving but noninteracting nucleons, with free-nucleon cross sections used for collisions between the incident particle and any individual bound nucleon. "Target-nucleon" momenta are chosen from a distribution which may depend on distance from the center of the nucleus, but not upon the stage of the reaction. Only one bound nucleon is assumed to be involved in each internal collision process, and neighboring nucleons do not share in the energy-momentum conservation of a particular nucleon-nucleon collision. Secondary α particles or deuterons cannot be predicted by the model in its current forms. Calculations generally assume a momentum distribution for the bound nucleons and a spatial dependence of the average nuclear potential which is appropriate to the nuclear size. Escaping particles are accumulated over a series of histories to sample the differential cross sections predicted by the model and to determine the excitation energy distribution of the residual nuclei. This residual excitation can be handled by a nuclear-evaporation or other model capable of dealing with redistribution of available energy to allow particle escape.

The most important conceptual requirements for the validity of the intranuclear-cascade model are that independent nucleon-nucleon reactions can occur sequentially within the nucleus and that decay of the nucleus does not have to be considered during the cascade phase of the reaction.

Classical kinematics are employed within the nucleus, so that the validity of cascade calculations depends on the wavelength of the incident nucleon being short enough for a single p-n or p-p interaction to be localized within, perhaps, $\sim 2\times 10^{-13}$ cm, the diameter of the region "occupied" by a bound nucleon. In considering the relation of the cascade model to the uncertainty relations, variables chosen at random should not be considered to be "sharp," even though the computer proceeds with machine precision. Thus the incident particles can be thought to have sharp momentum, and the localization of the collision point is related to the uncertainty in the scattered momentum, which has a possible range of values larger than the incident momentum itself. This broad uncertainty allows localization of a collision to a region about the size of $\lambda\!\!\!^{-}$ of the incident particle, 10^{-13} cm for a 20-MeV proton. Therefore, the assumption of a short incident wavelength is

[10] L. S. Azhgirey *et al.*, Nucl. Phys. **13**, 258 (1958).
[11] T. C. Randle *et al.*, Phil. Mag. **44**, 425 (1953).
[12] B. K. Nelson, G. Guernsey, and B. Mott, Phys. Rev. **88**, 1 (1952).
[13] P. H. Bowen *et al.*, Nucl. Phys. **30**, 475 (1962).
[14] A. K. Strauch and F. Titus, Phys. Rev. **103**, 200 (1956); **104**, 191 (1956).
[15] J. A. Hofmann and A. K. Strauch, Phys. Rev. **90**, 449 (1953).
[16] G. M. Temmer, Phys. Rev. **83**, 1067 (1951).
[17] N. S. Wall and P. R. Roos, Phys. Rev. **150**, 811 (1966); P. R. Roos, Ph.D. thesis, MIT, 1964 (unpublished).
[18] J. Genin *et al.*, J. Phys. Radium **22**, 615 (1961).
[19] P. Radvanyi and J. Genin, J. Phys. Radium **21**, 322 (1960).
[20] S. Dahlgren *et al.*, Arkiv Fysik **32**, 510 (1965).
[21] J. Hadley and H. York, Phys. Rev. **80**, 345 (1950).
[22] P. F. Cooper, Jr., and R. Wilson, Nucl. Phys. **15**, 373 (1960).
[23] W. N. Hess and B. J. Moyer, Phys. Rev. **101**, 337 (1956).
[24] M. L. Goldberger, Phys. Rev. **74**, 1269 (1948).
[25] N. Metropolis *et al.*, Phys. Rev. **110**, 185 (1958); **110**, 204 (1958).

not pressing, even down to nucleon energies in the nuclear-binding-energy region.

The comparisons with theory shown below were prepared using the cascade method and program of Bertini.[26] His standard model nucleus approximates the required nucleon density distributions in three radial steps, and has well depths chosen for each density region so that degenerate neutron and proton Fermi gases would have (in the correspondence-principle limit) the proper densities in each region if the minimum separation energies were 7 MeV. Table I lists the standard Bertini parameters used to produce the comparisons to be illustrated below. The potential well in Bertini's model is used to obtain the local kinetic energy outside the nucleus, but the well is not used to provide refraction of particles crossing the potential steps. The special assumptions of Bertini do not seem worse, in general, than those of the cascade model when his model is used for high-energy nucleons on heavy nuclides, but at the lowest secondary energies considered here, neglect of refraction and of details of the bound-nucleon-momentum distributions may be serious. Recent intranuclear-cascade calculations by Chen *et al.*[27] include refraction and also a density distribution with more steps.

To account for particle emission resulting from the residual excitation of the postcascade nucleus, Bertini[26] adapted the program written by Dresner[28] to carry out a Monte Carlo evaluation of the Weisskopf[29] evaporation processes in which enough excitation energy is available to produce more than one evaporated particle. Dresner followed the scheme of Dostrovsky *et al.*[30] For use with the cascade analysis, Bertini determined the postcascade nucleus and its excitation from each cascade Monte Carlo history; since the excitations were based on a fixed separation energy rather than nuclear-mass tables, energy was not quite conserved. Estimates of the evaporation cross sections for this paper were performed using a program of Aebersold, which differs for targets below $A=30$ from that originally employed by Bertini by including appropriate accumulated nuclear recoil kinetic energy and by using more accurate nuclear masses for nuclides away from the stability line. Except for the lowest energies and widest detector angles, the de-excitation of the postcascade nucleus is not very important for the proton-energy region above 20 MeV studied here, based on the small fraction of the measured cross sections predicted by this evaporation calculation. The conceptual weakness of the supposed sharp demarcation between the cascade and evaporation processes and of the many calculational approximations is therefore not important for comparisons given here.

TABLE I. Nuclear-model parameters for intranuclear-cascade calculations. These parameters, from the standard nuclear configuration of Ref. 26, were employed in the Monte Carlo calculations illustrated in this paper. The concentric boundaries between the regions of constant density are taken to be the same for neutrons and protons. The potentials and Fermi-gas densities given correspond to a 7-MeV separation energy for the least-bound nucleons.

Nuclide	Outer radius of region (10^{-12} cm)	Neutron Density (10^{36} cm^{-3})	Neutron Potential (MeV)	Proton Density (10^{36} cm^{-3})	Proton Potential (MeV)
^{9}Be	0.1114	64.4	−38.9	51.5	−34.5
	0.3000	31.8	−26.9	25.4	−24.2
	0.4744	3.68	−11.7	2.95	−11.1
^{12}C	0.1311	62.2	−38.2	62.2	−38.2
	0.3216	31.4	−26.8	31.4	−26.8
	0.4965	3.60	−11.7	3.60	−11.7
^{27}Al	0.2029	75.6	−42.5	70.2	−40.8
	0.3971	39.7	−30.1	36.9	−29.0
	0.5721	4.47	−12.4	4.15	−12.1
^{59}Co	0.2973	87.5	−46.1	73.8	−42.0
	0.4926	47.2	−33.0	39.9	−30.2
	0.6676	5.27	−13.0	4.45	−12.4
^{209}Bi	0.5156	106.9	−51.8	70.4	−40.9
	0.7111	59.3	−37.2	39.1	−29.9
	0.8862	6.61	−14.0	4.36	−12.3

While the present work suffered from poor energy resolution, poor statistical accuracy, and lack of particle discrimination, it did produce spectra down to 20 MeV at a wide range of angles for targets other than carbon. Details of the experiment and of the supporting calculations are available.[31] The results bear on the range of validity of the simple quasifree-scattering model and its elaborations through the cascade-plus-evaporation model.

II. APPARATUS

The experiment employed an air-mounted flight-time spectrometer based on the use of plastic scintillators. Before striking targets about 0.6 g/cm^2 thick, 160-MeV protons from a beam with an intensity of 5×10^4 protons/sec passed through timing counters A and A′ operating in a 2-nsec coincidence. Scattered charged particles were detected by a coincidence telescope consisting of a 0.5-mm counter (C′) and a 12-mm counter (B′), 10 and 12 cm in diam, respectively. The flight time was measured between the pulse in B′ and the delayed pulse from counter A, and was recorded if there was an AA′B′C′ delayed coincidence and if no other beam proton was sufficiently close in time for confusion to occur.

The available 1-nsec time resolution could not give reasonable energy resolution at the higher energies with the 90-cm flight path used for scattering angles of 10° and 30° or the 70-cm path used for larger angles. At low

[26] H. Bertini, Phys. Rev. **131**, 1801 (1963); Oak Ridge National Laboratory Report No. ORNL-3383, 1963 (unpublished).
[27] K. Chen *et al.*, Phys. Rev. **166**, 949 (1968).
[28] Lawrence Dresner, Oak Ridge National Laboratory Report No. ORNL-CF-61-12-30, (1961) (unpublished).
[29] J. M. Blatt and V. F. Weisskopf, *Theoretical Nuclear Physics* (John Wiley & Sons, Inc., New York, 1952), pp. 365ff.
[30] I. Dostrovsky *et al.*, Phys. Rev. **116**, 683 (1959); **118**, 781 (1960); **118**, 791 (1960).
[31] R. W. Peelle *et al.*, Oak Ridge National Laboratory Report No. ORNL-3887, 1966 (unpublished).

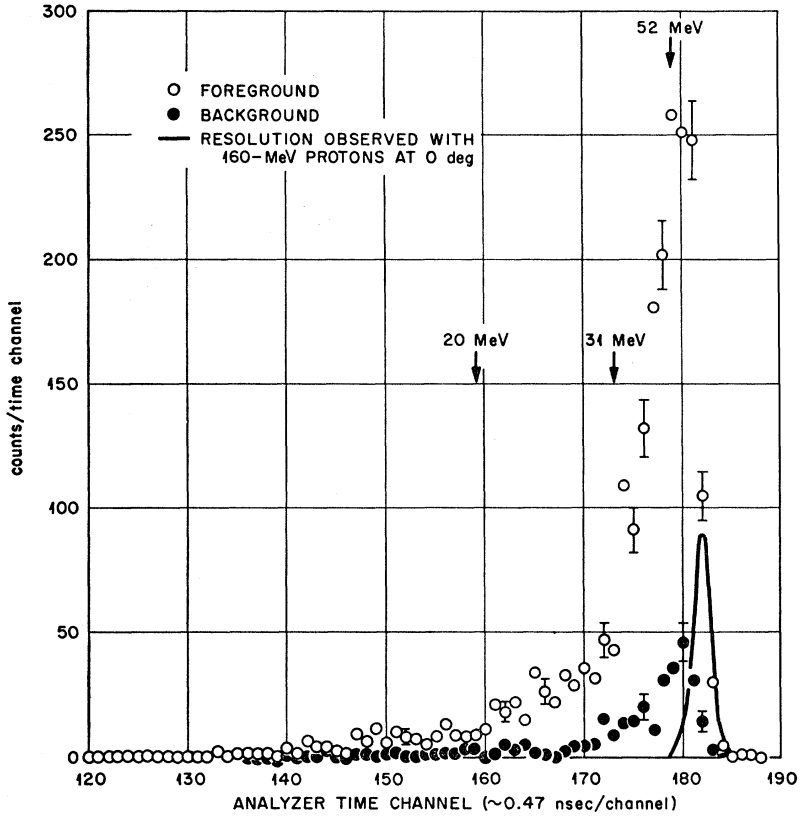

FIG. 1. Raw pulse-height spectra from the time-to-pulse-height converter for secondary charged particles, at 30° from a 0.7-g/cm² Co target, along with the corresponding background. The solid curve shows the resolution function in the unscattered beam.

secondary energies, the spectrometer sensitivity was reduced by energy loss in its components; a proton leaving the target with 13 MeV could just be detected in counter B′ above its threshold of 4 MeV. If this proton had originated in a reaction at the side of the target farthest from the detector, it would have started with about 25 MeV.

The properties of the beam of the Harvard University Synchrocyclotron have been described in some detail elsewhere.[32] The proton beam had an energy of 158±1 MeV at the center of the target, which absorbed in the various cases between 3 and 5 MeV. The 12-mm beam spot changed its position an average of about 1 mm during the one-day intervals between adjustment. About 30% of the incident protons were disregarded because they occurred within 110 nsec of another proton, as a result of the cyclotron's ~2% duty factor. This timewise isolation of the beam protons was enforced using logic circuits described by Hill *et al.*[33] in the system described in Ref. 31.

The spacing between counters B′ and C′ of the secondary proton telescope ranged between 30 and 50 cm. This distance was chosen to make negligible the detection of uncharged particles via reactions in one of the counters. The threshold of detector C′ was adjusted so that it did not affect the telescope efficiency, and the $2\tau = 24$-nsec resolving time of the B′C′ coincidence circuit was set to assure coincidence efficiency above 98% for protons of all pertinent energies. Unfortunately, energetic deuterons did register in the spectrometer at about half their actual energy.

The angular resolution of the secondary-particle telescope was governed by the detector geometry and by multiple Coulomb scattering in the target. The geometrical rms angular resolution of 0.03 rad was exceeded by the rms-projected multiple Coulomb scattering contribution for only the lowest energies for light targets, but for all energies below 40 MeV for cobalt and below 50 MeV for bismuth targets. In the last case, the rms angular resolution became 0.13 rad at 20 MeV. This spreading was not considered serious, because the nuclear scattering cross sections become more isotropic for low secondary energies.

Count losses, reactions in the target and the secondary telescope, coincidence losses, and multiple Coulomb scattering in detector C′ reduced the telescope efficiency to between 0.95 and 0.98 for protons leaving the target reaction point in the direction of the B′ detector. An energy-dependent efficiency correction was introduced.

Flight-time measurements were obtained from a time-to-amplitude converter calibrated against delay cables and absolute random-coincidence rates. "Zero" flight

[32] R. T. Santoro, Oak Ridge National Laboratory Report No. ORNL-3722, 1964 (unpublished).
[33] N. W. Hill *et al.*, Oak Ridge National Laboratory Report No. ORNL-3687, 1964 (unpublished).

time was deduced from observation of the apparent flight time of beam protons, with detector B′ placed at 0°, using a beam intensity of about 500 protons/sec. The conversion gain was stable within 0.5%, but over-all shifts in the timing zero corresponded to 0.2–0.3 nsec. Over the useful part of the flight-time spectrum, the amplitude of the signals in counter B′ varied by 10:1; so time-slewing corrections were performed based on measurements in the degraded 160-MeV proton beam and upon later measurements using neutrons from the $T(d,n)\alpha$ reaction timed by the associated α particles.[34] The resulting slewing corrections ranged up to 1.5 nsec.

Table II lists the uncertainties in the experimental parameters.

III. DATA ANALYSIS

A. Backgrounds

Figure 1 shows a typical experimental flight-time spectrum with its associated target-out background, before the counts in neighboring time channels were combined into bins whose widths depended on the energy resolution. The target-out backgrounds for detector angles of 30°, 45°, and 120° were dominated by air scattering, while at 60° and 90°, the target holder was rotated so that it produced additional scattering. At 10°, the background was dominated by scattering in the beam counters A and A′. In the worst case, the measured relative background amounted to 15% of the counts. Background contributions from twofold scattering in the target were not carefully analyzed, but amounted to 1–3%.

B. Energy Calibration

Secondary protons lost a variable amount of energy in the target and then penetrated six successive material regions before being detected in detector B′. A digital-computer program produced the bin-response functions $N_k(E)$, which give the probability that a proton born in the target at energy E and headed toward the detector's sensitive area would have been detected in the kth time bin.

TABLE II. Estimated standard errors for experimental parameters which entered into the data analysis. Where no range of values is indicated, the same estimates were used for all runs.

Beam energy	±1.0 MeV[a]
Detector area	0.4%
Detector efficiency	1.5%
Time-slewing correction	0.25 of correction relative to 158 MeV
Time-to-amplitude conversion factor	1%
Zero of timing scale	0.1–0.25 nsec
Scattering angle	0.5°
Flight path on center line	0.3 cm
Lateral-beam-spot position	0.15 cm
Surface density of secondary-proton telescope	1.5 mg/cm²
Number of protons striking target	1–2%
Surface density of target	0.3–1.5% for metal targets 3.5% for the water target
Angle of target normal	0.5°

[a] From measurements reported in R. T. Santoro, Oak Ridge National Laboratory Report No. ORNL-3722, 1964 (unpublished).

[34] T. A. Love *et al.*, Oak Ridge National Laboratory Report No. ORNL-3893, 1966 (unpublished).

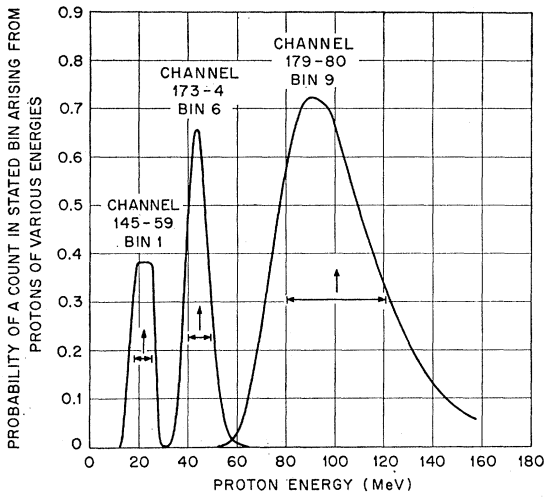

FIG. 2. Typical response functions $N_k(E)$ for the flight-time spectrometer (90-cm flight path).

The incremental energy-loss calculations which made the computation complex were performed according to a procedure[35] involving interpolation of "shell corrections" from a graph by Turner.[36] The response-function computation averaged the actual flight time of secondary protons from various parts of the target and also took into account statistical timing fluctuations, time slewing, and the width of the time bins into which the counts were collected. The $N_k(E)$ functions were normalized so that $\sum_k N_k(E)=1$ for all E above that required for a proton to be detected if it originated at a point in the target most distant from the detector. The $N_k(E)$ yielded the energy resolution of the system, the energy integral $\int_E N_k(E)dE$ was taken as the energy width Δ_k of the kth time bin, and the resulting cross sections from bin k are plotted at the mean energy $\bar{E}_k \equiv \int_E E N_k(E)dE/\Delta_k$.

Figure 2 shows typical response functions $N_k(E)$ computed for the 90-cm flight path. *A priori* information about the proton spectrum's upper energy limit was included in the response functions and therefore in the bin parameters derived from them, a procedure important and useful for the highest-energy bins. Figure 3 illustrates a few sections through the response surface for constant E, each of which represents a spectrum that would have been observed for monoenergetic protons. For plotting in Fig. 3, the computed intensity in each bin was divided by the bin width Δ_k and plotted

[35] R. W. Peelle, Oak Ridge National Laboratory Report No. ORNL-TM-977, 1965 (unpublished).

[36] J. E. Turner, Ann. Rev. Nucl. Sci. **13**, 1 (1963).

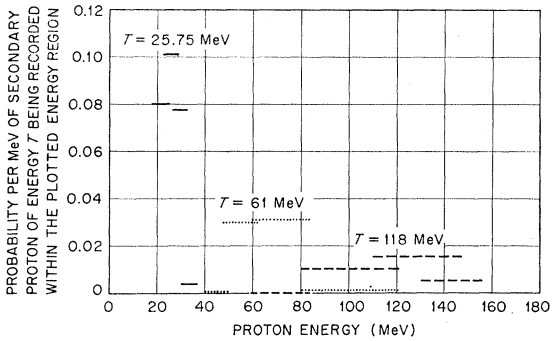

FIG. 3. Computed response of the proton flight-time spectrometer (90-cm flight path) to monoenergetic protons of three energies.

as a bar covering the energy range $\bar{E}_k \pm \sigma_k$, where σ_k is the standard deviation of $N_k(E)$.

The integral cross sections above the spectrometer's lower-energy limit, obtained by summing the counts in all bins, correspond to a response function which is unity above a linear cutoff in the 20-MeV region induced by effective thinning of the target.

The counts in time bin k yielded a differential cross section which was an average weighted by $N_k(E)$. The desired integral properties of these average cross sections are guaranteed by the unit normalization of $\sum_k N_k(E)$.

C. Uncertainties

To understand the implications of the uncertainties listed in Table II, a first-order error analysis was performed. Correlations among the experimental variates were taken into account. The target thickness, for example, affects both the number of scattering centers and the width of the energy bins. At the suggestion of R. L. Cowperthwaite, the required partial derivatives of the cross sections with respect to the experimental variates were obtained with the help of a simplified energy-calibration analysis and the implicit function theorem.

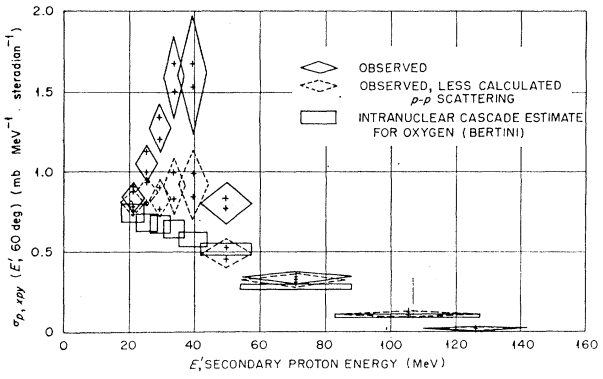

FIG. 4. 158-MeV protons on H_2O, 60° scattering. Oxygen cross sections are shown from Bertini's intranuclear-cascade calculation and from a subtraction of estimated p-p scattering from the experimental data.

Uncertainties in the normalization of secondary differential-energy spectra amount to 3–4%, except when water targets were used. The energy-calibration uncertainty ranged from 1 to 10%, with a maximum absolute uncertainty of 5–6 MeV in the region of 100 MeV. Drift in the timing zero and uncertainty in the time-slewing correction were the dominant contributions. The resulting bin-width uncertainty made a major contribution to cross-section uncertainty for particular time bins, but had little effect on integral cross sections. For this reason, the data plots show both statistical standard errors and errors combined from all sources.

IV. RESULTS

A. Scattering of Protons from Hydrogen

Figure 4 illustrates the laboratory-system cross section observed at 60° from a water target, where the

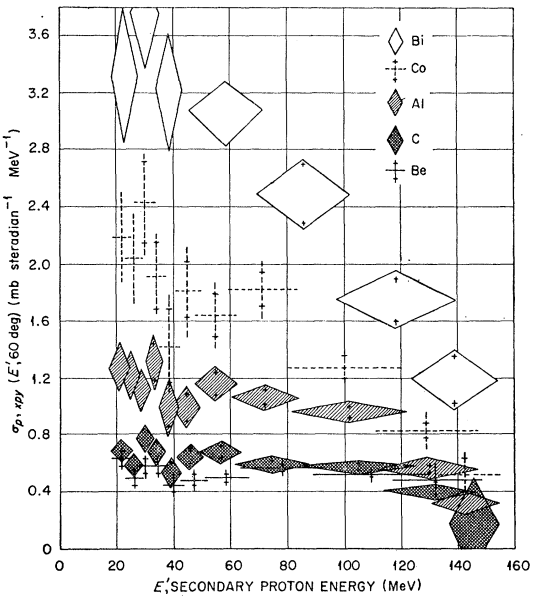

FIG. 5. Secondary-proton differential cross sections at 30° for 158-MeV protons on various elements. The full energy width of each symbol is twice the standard deviation of the bin-response function, and the symbol is centered at the mean bin energy. The inner uncertainty value on each cross section is from counting statistical uncertainties alone, while the outer one includes all other error sources.

p-p scattering should appear at 37 MeV. The data do show a prominent excess over those predicted for oxygen alone in an intranuclear-cascade calculation. The hydrogen-scattering contribution subtracted from the data in preparing Fig. 4 was based on a p-p c.m. differential cross section of 3.7 ± 0.1 mb/sr, and was broadened by a resolution function which combined the $N_k(E)$ with the variation of the energy of hydrogen-scattered protons over the angular opening of the spectrometer. The position of the experimental peak appears

correct within the assigned energy standard error of 2 MeV. The magnitude of the experimental peak appears perhaps 10% too large, although the comparison is imprecise, because the oxygen cross section was not measured and because the target thickness was poorly known. Figure 4 shows that the system was reasonably calibrated in energy and efficiency, at least in the 40-MeV region.

Scattering from H_2O and D_2O targets at 30° was also observed, but the energy resolution was too coarse above 70 MeV to allow the effects of hydrogen to be separated from those of oxygen. The data suggested an oxygen cross section about as large as the cross section observed for aluminum.

B. Angle-Energy Differential Cross Sections for Protons on Nuclei

In this section, the observed laboratory differential cross sections are illustrated, along with comparisons

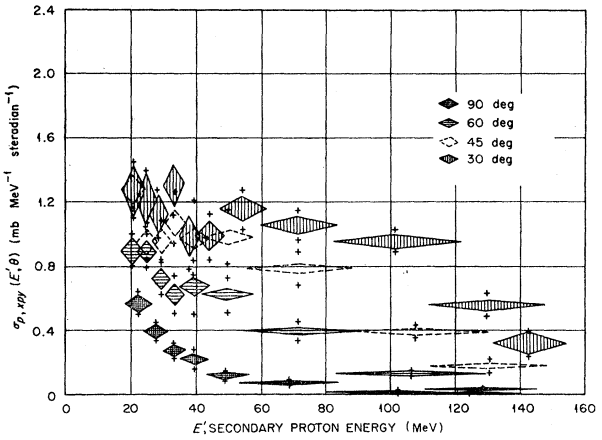

FIG. 6. Secondary-proton spectra from Al at various angles.

with those observed in other experiments and with the intranuclear-cascade model.

Figure 5 shows the cross section observed at 30° for various targets, ranging from beryllium through bismuth. The cross sections increase monotonically with atomic weight, and at the available resolution there is no structure. The cross sections are less flat for the heavier nuclei, presumably because two- and three-step intranuclear cascades are more common there. The available comparisons at larger angles are consistent with the same relative behavior versus mass number shown in Fig. 5.

Figures 6 and 7 illustrate the observed differential cross sections for aluminum and cobalt, respectively. The spectra become softer with increasing angle, as would be expected if nucleon-nucleon encounters within the nucleus dominate the reaction mechanism.

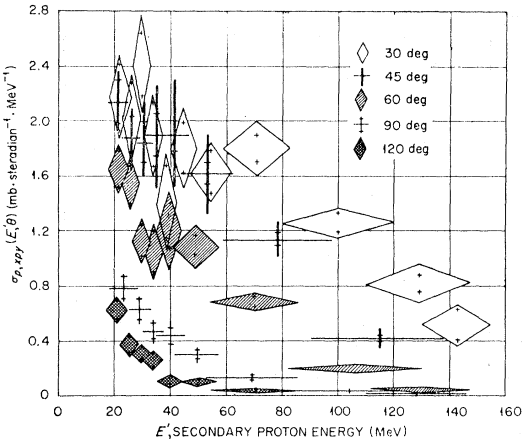

FIG. 7. Secondary-proton spectra from Co at various angles.

Few experiments have produced data directly comparable to those shown here. Wachter *et al.*[37] observed spectra at 60° for protons above 50 MeV from Al and Co which seem to agree with those shown in Figs. 6 and 7 within stated errors, except at the lowest and highest energies. There is serious disagreement with the data of Wall and Roos,[17] who found markedly more intensity than we did at the high end of the spectra and a decreasing cross section down to their 40-MeV cutoff, even for angles above 50°. Figure 8 shows the only case for which a nearly direct comparison of all three experiments is possible. Data from nickel obtained by Wall and Roos are compared to cobalt data for the other experiments, permissible because both sets of data show a very small change in the observed spectra with target

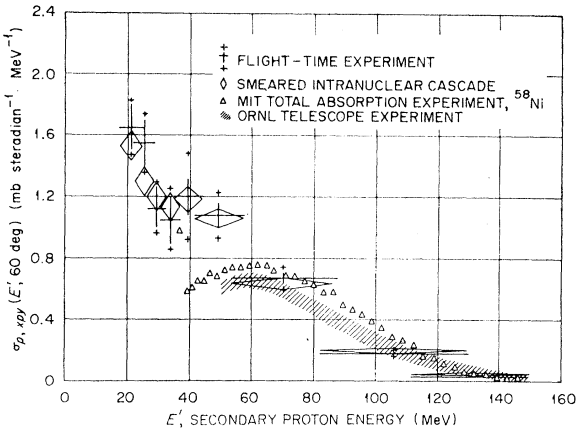

FIG. 8. Differential cross sections for 158-MeV protons from Co at 60°. Data from this experiment are compared with those of Gibson, with intranuclear-cascade estimates of Bertini, and with the experiment of Wall and Roos (Ref. 17) for Ni. The theoretical estimates have been smeared with the computed instrument response. (The Wall-Roos data are from the Roos thesis and have not been corrected for the multiple scattering described in the later paper.)

[37] J. W. Wachter *et al.*, Phys. Rev. **161**, 971 (1967); also, National Aeronautics and Space Administration Report No. NASA-SP-71 (1964), p. 337 (unpublished).

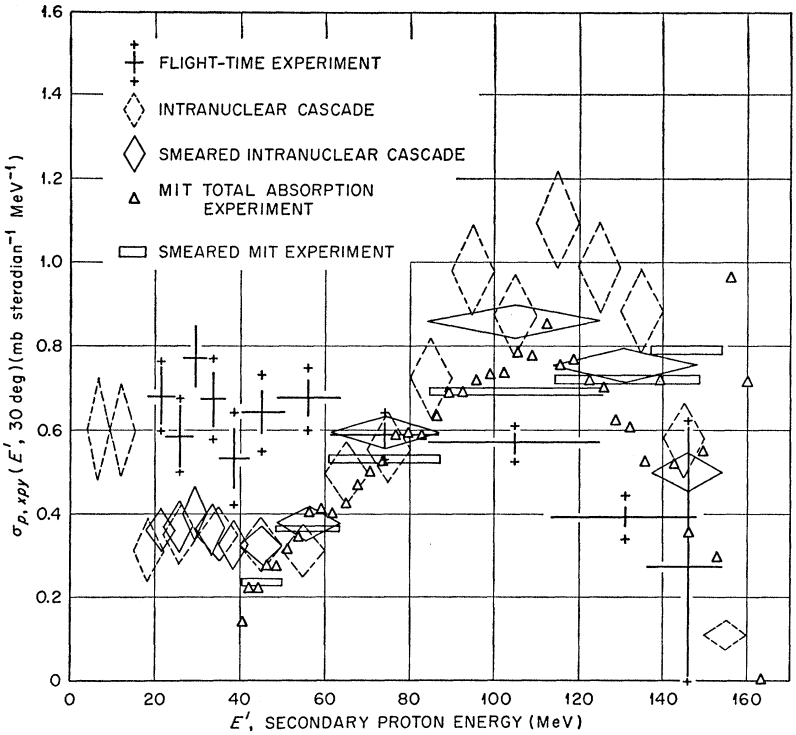

FIG. 9. Differential cross sections at 30° for protons from 158-MeV protons on Co. Comparisons with the experiment of Wall and Roos (Ref. 17) and with the intranuclear-cascade estimates of Bertini are exhibited with and without resolution smearing according to the calculated detector-response functions.

mass number. With or without correction to include our much larger instrumental broadening, the Wall-Roos data lie well above ours above 60 MeV and below it at lower energies. Figure 9 shows a comparison at 30° for a carbon target, typical of the observed discrepancies between the Wall-Roos data and ours for Be and Bi and for Ni-Co as well. Presumably, the relatively low cross sections observed in this experiment at high secondary energies could be explained if the resolution functions

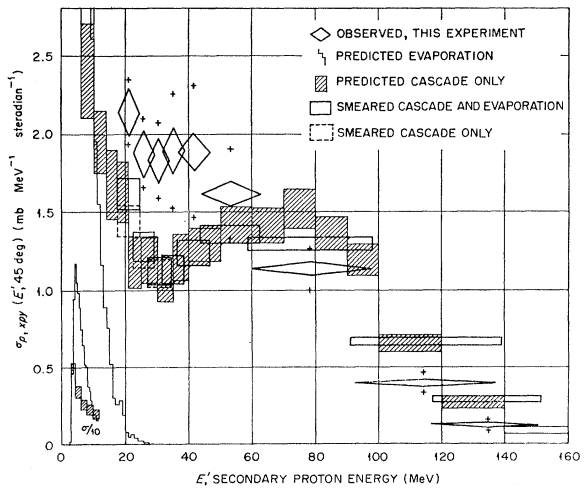

FIG. 10. Differential cross sections at 40° for protons from 158-MeV protons on Co. Experimental points are compared with the histogram representing the Bertini cascade and evaporation estimates, and with the estimates as smeared by the detector resolution. The effect of the (assumed) isotropic evaporation contribution on the smeared spectrum is shown.

estimated here are too narrow, though in the 160-MeV region there is the most information on which to base the resolution estimates. The even stronger disagreement at 40–60 MeV is not fully explicable; the approximately correctly observed p-p scattering strongly supports the results of this paper, since a hypothetical shape error in the spectra here would have to be associated with a considerable energy and intensity error in the position of the p-p peak in Fig. 4. Part of the 40- to 60-MeV discrepancy can be explained by our detection of ~100-MeV deuterons there.

The recent work of Brun *et al.*[38] includes data for 156-MeV proton on gold and silver targets. They did not see the decrease in cross section at low energy reported by Wall and Roos,[17] but their results for gold at 25° do not rise as high at low energies as do our 30° bismuth data in Fig. 5.

The cross sections for 185-MeV protons given by Dahlgren *et al.*[20] for angles of 60°–100° are slightly larger than those shown in Figs. 6 and 7, but their shapes are just within our uncertainties.

Figure 8 illustrates that our experiment is in good accord with the Bertini intranuclear-cascade estimates at 60°. Using the cross sections for protons at 45° from a Co target, Fig. 10 illustrates another typical comparison of the present data with the cascade-plus-evaporation calculations of Bertini. The importance of the evaporation estimate is indicated, along with the typical effect of smearing the estimates using the computed $N_k(E)$, to allow direct comparison with experiment. The

[38] C. Brun *et al.*, Nucl. Phys. **A95**, 337 (1967).

TABLE III. Angle differential laboratory cross sections for secondary protons above ~20 MeV, compared with available estimates.

Target	Angle (deg)	Energy cutoff (MeV)[a]	$\sigma_{p,xpy}(\theta)$ (mb/sr) Meas	Est	Decomposition of estimated $\sigma(\theta)$ (mb/sr) Elastic[b]	Cascade[c]	Evaporation[d]
Be	30	20.1	70 ± 2	68 ±1.5	3	64.3 ±1.4	0.73±0.03
C	10	20.0–59	32.5± 2.3	9.7 ±1.2	···	9.2 ±1.2	0.53±0.04
	30	19.9	75 ± 3	90 ±3	3	86.4 ±2.3	0.54±0.04
Al	10	19.6–59	65 ± 4	23 ±2	···	22.8 ±1.5	0.67±0.03
	30	19.5	124 ± 4	133 ±3	7	125.2 ±2.3	0.68±0.03
	45	19.2	80 ± 3	85.7 ±1.6	~0.5	84.4 ±1.6	0.77±0.03
	60	19.2	43 ± 1.5	45.0 ±1.1	~0.04	44.2 ±1.1	0.77±0.03
	90	20.7	11.4± 0.6	8.2 ±0.4	~0	7.6 ±0.4	0.63±0.03
Co	10	19.9–61	82 ± 7	39.7 ±2.4	···	38.9 ±2.4	0.82±0.05
	30	20.0	187 ± 7	196 ±3	7	188 ±3	0.82±0.05
	45	19.2	128 ± 5	130 ±2.3	~0.5	128.2 ±2.3	1.02±0.05
	60	19.3	70 ± 3	67.5 ±1.6	~0.05	66.5 ±1.6	1.00±0.06
	90	20.9	21.2± 1.1	13.0 ±0.6	~0	12.2 ±0.6	0.79±0.05
	120	19.7	9.7± 0.7	3.35±0.2	~0	2.38±0.17	0.97±0.06
Bi	10	18.6–62	126 ±20	57 ±3	···	55 ±4	1.6 ±0.1
	30	18.7	330 ±14	269 ±5	15	252 ±5	1.5 ±0.1

[a] Taken for one-half maximum sensitivity on the integral response function for all bins summed.
[b] Uncertainties in the estimated elastic scattering are taken as 10%, except in Co, O, and Bi, where they are 15–20%.
[c] The angular intervals generally used in sorting the Monte Carlo output were 0°–14°, 24°–35°, 40°–50°, 56°–64°, 85°–95°, and 110°–131°. The 30° interval for carbon was 21°–38°. The uncertainties indicated arise from Monte Carlo statistics alone.
[d] The quoted uncertainties are of statistical origin. Fairly small changes in the evaporation model described in Sec. V can produce up to 10% changes.

observed spectrum is softer, showing no quasifree-scattering peak. This contrast was slightly less marked for Al at 45°. The Bertini predictions at 30° for all nuclides show a broad peak near the energy corresponding to quasifree scattering, while Fig. 5 shows that an unpeaked shape is characteristic of all the data obtained here. Figure 9 shows the contrast for carbon; the difference is slightly less pronounced for heavier nuclides. Smearing the Bertini estimates with the calculated $N_k(E)$ does not markedly affect the disagreement. The recent intranuclear-cascade calculations of Chen *et al.*[27] indicate that the cross-section peaking near the quasifree-scattering energy is reduced in his calculation by the inclusion of refraction effects.

C. Integrals over the Energy Spectra

Table III gives the integrals of the observed cross sections over the proton-energy region above about 20 MeV, as obtained by summing contributions from all the energy bins. (The data obtained at 10° are shown only for the 20 to 60-MeV interval, within which the elastically scattered protons can have no effect.) The integrated cross sections at 30° rise slightly more slowly than the nuclear area, but if divided by $A^{2/3}$, the Co and Al integrated cross sections agree within about 10%. If the Co data are integrated over angle and energy, one obtains σ ($E>20$ MeV, Co)$\cong$0.68 b.

Estimated integrated cross sections above 20 MeV are compiled in Table III from the intranuclear-cascade, evaporation, and elastic scattering contributions. The elastic scattering cross sections were based on estimated optical-model parameters[39] whose accuracy was assessed by comparison with the data of Roos and Wall.[40] The intranuclear-cascade estimates are seriously low at 90° and 120°, but at scattering angles (30°–60°) where the energy is split rather evenly in the initial intranuclear encounter, the integral agreement is generally very good. The disagreements at 30° for Bi and C are puzzling.

V. CONCLUSIONS

The comparisons with the cascade-plus-evaporation theory are encouraging. The general agreement of the angle and energy distributions is taken by us to imply the approximate validity of the cascade model at these energies. No statement can be made about the evaporation contribution because it is so small.

There are two areas of consistent disagreement with the Bertini calculations:

(1) Estimates at back angles are far too small. Back-angle scattering would be increased by any failure of the notion that the target nucleons see only the average potential. Further, the estimated average excitation energy remaining with the nucleus after the cascade process is enough (50 MeV for Co) to affect the back-angle cross sections if the evaporation theory is badly in error for transitions to levels near the ground state. This is the region of the evaporation theory's greatest conceptual weakness. Modification of the theory along the line suggested by Griffin[3] would be pertinent.

(2) At angles through 45°, the Bertini estimates give less intensity than our experiment at energies below 50 MeV or so, as well as quasifree-scattering peaks which are much more marked. (The data of

[39] R. M. Haybron (private communication). (As in G. R. Satchler and R. M. Haybron for radius parameter and general technique, but 5–10% greater in magnitude for the potential parameters.)

[40] P. R. Roos and N. S. Wall, Phys. Rev. **140**, 1237 (1965).

Wall and Roos[17] disagree with ours.) These differences could arise from failures in the basic model assumptions or could represent the effect of neglected distortions produced by the average potential. The validity of our data in the 40-MeV region is supported by the results for the water target but is weakened by the failure of the experiment to differentiate between various secondary charged particles.

This experiment supports the hypothesis that continuum cross sections are predictable by some intranuclear-cascade model down to energies where the proton wavelength λ is about the size of a target nucleon. From limited data, the model seems as applicable to light nuclides as to medium-weight ones. These tentative findings could be illuminated by going to lower energies in both incident and secondary particles, by studying the back angles more carefully, by measuring at enough angles to allow reasonable integrals over solid angle, and by clearly identifying the particle type of all secondaries.

ACKNOWLEDGMENTS

We are indebted to A. M. Koehler and his crew for helping us utilize the Harvard University Cyclotron, and to the U. S. Office of Naval Research for supporting the costs of our machine use. We thank R. L. Cowperthwaite and P. M. Aebersold for extensive help in analysis and computation, and Hugo Bertini for his many explanations of cascade-plus-evaporation theory and practice. We depended upon Floyd Glass for the design of a stable time-to-amplitude converter, upon Vern McKay and Hugh Brashear for the design of detectors, upon T. Sliski for the mechanical apparatus, and upon support personnel for their careful assistance.

PHYSICAL REVIEW VOLUME 167, NUMBER 4 20 MARCH 1968

Measurements and Distorted-Wave Born-Approximation Analyses of Some 13.9-MeV Differential Cross Sections for the $N^{14}(He^3,\alpha)N^{13}$ Reactions*

B. T. LUCAS,† D. R. OBER, AND O. E. JOHNSON
Department of Physics, Purdue University, Lafayette, Indiana
(Received 19 October 1967)

The (He^3,α) differential cross sections leading to the ground and 2.367-, (3.51+3.56)-, 6.38-, and (7.18+7.42)-MeV states of N^{13} have been measured at an incident He^3 energy of 13.9 MeV using silicon surface-barrier detectors and a conventional electronic spectrometer system. Energy spectra were accumulated at 2.5° intervals over a laboratory angular range 17.5°–90° and at 5° intervals from 90° to 170°. The experimental differential (He^3,α) cross sections corresponding to states in N^{13} at 0, 2.367, 6.38, and (7.18+7.42) MeV exhibit a pronounced oscillatory structure, suggesting that a direct-reaction mechanism is dominant. The composite cross section corresponding to the transitions leading to the (3.51+3.56)-MeV doublet has a somewhat washed-out structure. All angular distributions display a definite forward-angle peaking, and those leading to the ground and 2.367- and (3.51+3.56)-MeV states of N^{13} show evidence of strong backward-angle peaking. The transitions leading to the odd-parity states in N^{13} appear to be considerably enhanced relative to those leading to the even-parity states. The angular distributions corresponding to the transitions to the ground and 2.367- and 6.38-MeV states have been analyzed within the framework of the zero-range distorted-wave theory using a simple knockout model. The use of cutoff radii equal to or slightly larger than the nuclear radius was necessary in order to obtain reasonably good representations of the experimental data.

I. INTRODUCTION

IN several previous investigations of the $N^{14}(He^3,\alpha)N^{13}$ reactions,[1–3] it was observed that the differential cross section for producing the negative-parity ground state of N^{13} is considerably greater than that for the production of the positive-parity state at 2.367 MeV. Furthermore, in two of these studies,[1,2] it was found that the composite differential cross section corresponding to the unresolved α-particle groups associated with the closely spaced (3.51+3.56)-MeV doublet in N^{13} is approximately equal to that for producing the ground state. The results from less complete studies[4,5] at other energies, in which the cross sections were measured at

* Work supported in part by the U. S. Atomic Energy Commission.
† Present address: 1713 Myrtle Avenue, Whiting, Ind.
[1] I. J. Taylor, F. de S. Barros, P. D. Forsyth, A. A. Jaffe, and S. Ramavataram, Proc. Phys. Soc. (London) A75, 772 (1960).
[2] K. P. Artemov, V. Z. Goldberg, B. I. Islamov, V. P. Rudakov, and I. N. Serikov, Yadern. Fiz. 1, 1019 (1965) [English transl.: Soviet J. Nucl. Phys. 1, 726 (1965)].
[3] A. R. Knudson and F. C. Young, Bull. Am. Phys. Soc. 12, 502 (1967).
[4] A. Gallmann, D. E. Alburger, D. H. Wilkinson, and F. Hibou, Phys. Rev. 129, 1765 (1963).
[5] T. E. Young, G. C. Phillips, R. R. Spencer, and D. A. A. S. N. Rao, Phys. Rev. 116, 962 (1959).